Asymmetric Vortex Wake Development on Missiles at High Angles of Attack

F. D. Deffenbaugh* and W. G. Koerner†
TRW Defense and Space Systems Group, Redondo Beach, Calif.

An analysis of recent wind-tunnel results is presented describing the influence of Mach number, Reynolds number, and body geometry on asymmetric vortex development and associated forces on slender missile configurations at high angles of attack. Experimental force and moment coefficients, load distributions, and surface-pressure distributions (steady and unsteady) are presented for several ogive and triconic nose configurations for angles of attack up to 90°, subsonic to low supersonic Mach numbers, and Reynolds numbers (based on body diameter) from 3.17×10^5 to 3.17×10^6. Asymmetric vortex locations and strengths, boundary-layer separation lines, and side-force coefficients are predicted using the unsteady cross-flow analogy and a discrete vorticity cross wake. Predictions of side force coefficients compare well with the force test data for angles of attack up to 40°.

Nomenclature

A = base area $= \pi d^2/4$
a = circular cylinder radius
CN = normal-force coefficient $= N/\frac{1}{2}\rho V^2 A$
CY = side-force coefficient $= Y/\frac{1}{2}\rho V^2 A$
C_p = equivalent-pressure coefficient $= (p-p_\infty)/\frac{1}{2}\rho u_m{}^2$
c_ℓ = unsteady sectional side-force coefficient $= -4/\pi\frac{1}{2}\int_0^{2\pi}\bar{p}/\frac{1}{2}\rho V^2 \sin\theta r d\theta$
c_n = sectional normal-force coefficient $= 4/\pi\frac{1}{2}\int_0^{2\pi} c_p \cos\theta r d\theta$
c_y = sectional side force coefficient $= -4/\pi\frac{1}{2}\int_0^{2\pi} c_p \sin\theta r d\theta$
c_p = pressure coefficient $= (p-p_\infty)/\frac{1}{2}\rho u_m{}^2$
$(\Delta C_p)_{\rm rms}$ = root mean square of test section freestream pressure fluctuation
d = cylindrical after-body diameter
ℓ = total body length
ℓ_n = nose length
M = Mach number
n = frequency of shedding of vortices of like sign
N = normal force
r = local body radius
r_n = nose radius
Rd = Reynolds number based on body diameter $= Vd/\nu$
Rc = cross-flow Reynolds number $= Rd\sin\alpha$
Rtr = transition Reynolds number $= \bar{x}u_{tr}/\nu$
(r,θ) = polar coordinates
S = cross-flow Strouhal number $= nd/U$
t = nondimensional time $= Ut(\text{sec})/a$
U = cross-flow velocity
u = outer-flow velocity evaluated at the cylinder surface
u_m = maximum velocity $= u(x_m)$
u_{tr} = velocity at transition $= u(x_{tr})$
V = freestream velocity
(x,y,z) = missile coordinate system, z = axial distance measured from missile nose apex
$\bar{x}$ = Stratford equivalent distance around two-dimensional circular cylinder
$\bar{x}$ = distance around cylinder surface from $\theta = 0°$
$\bar{x}_m$ = point at which maximum velocity occurs
$\bar{x}_s$ = forward stagnation point
$\bar{x}_{tr}$ = point of boundary-layer transition
Y = side force
Z_n = extent of laminar boundary layer aft of missile nose apex
α = angle of attack
Γ = circulation

Received June 30, 1976; presented as Paper 76-364 at the AIAA 9th Fluid and Plasma Dynamic Conference, San Diego, Calif., July 14-16, 1976; revision received Oct. 13, 1976.

Index categories: LV/M Aerodynamics; Jets, Wakes, and Viscid-Inviscid Flow Interactions; Boundary Layers and Convective Heat Transfer—Turbulent.

*Head, Aero-Analysis Section. Member AIAA.
†Aerospace Engineer.

Introduction

PRIOR to the current air slew missile, and ballistic missile air launch concepts, missile designers were primarily concerned with flight at small angles of attack. Wind-tunnel tests, empirical theories, and inviscid slender-body theories provided enough aerodynamic information for conventional tactical or ballistic missile design.

For angles of attack above 5°-7°, the flow on the lee side of a missile separates and rolls up into regions of concentrated vorticity. With increasing angle of attack, large side forces and moments and large dynamic loads may occur as a result of asymmetric vortex formation and vortex shedding. For air slew missiles, or any missile configuration that encounters large angles of attack where flow separation occurs, linear inviscid theory is inapplicable, and no complete viscous theory exists describing the complicated three-dimensional flow field.

Wind-tunnel investigators show that a large variety of vortex flows may be encountered, depending on at least the angle of attack, particular flow conditions, and body geometry. Although investigators generally agree that increasing Mach number, decreasing nose fineness, and a slight nose bluntness reduce side force, existing experimental data have led to conflicting and often confusing results concerning the effect of Reynolds number on side force. In addition, most of the available information is for tangent ogive or conical nose shapes. The effect of other nose geometries, such as triconic shapes, on side force has not been resolved.

The objective of the current wind-tunnel investigation is to provide design information for an air-launched ballistic missile encountering very large angles of attack during the launch transient. In addition to the experimental study, an

analytic method was developed using the unsteady cross-flow analogy to predict the flowfield about slender missile configurations for angles of attack up to 40°. The asymmetric wake in the cross-flow plane is described by a large number of discrete point vortices. For high Reynolds number flow, Stratford's turbulent separation criterion is used to specify the location at which point vortices are fed from the boundary layer into the wake.

Description of Experiment

Test Facilities

The aerodynamic data presented were obtained from wind-tunnel tests conducted in the 16-ft Propulsion Wind Tunnel (PWT) at Arnold Engineering Development Center (AEDC). PWT 16T has a 16×16 ft test section and operates within a Mach number range of 0.20 to 1.60 and within a unit Reynolds number range of approximately 0.50×10^6-6.0×10^6 ft.$^{-1}$

In order to traverse the 180° angle-of-attack regime, a conventional sting support was used for the range $-5°<\alpha<45°$ ($+5°<\alpha<55°$ during Phase III pressure tests) and a side-mounted strut support was used for the range $40°<\alpha<180°$.

Models

The tests were completed in four parts: a force test and Phase I, II, and III pressure tests. The model configurations are presented in Fig. 1. Separate pressure and force models were used in the investigation. The pressure model was instrumented with up to 260 pressure orifices for configuration N2B1, and the data were obtained by seven internally mounted 48-port Scanivalves and seven strain gage pressure transducers. Unsteady pressure data were taken during the first and second phases of the pressure tests. Microphones were located at four stations along the body, eight at each station arranged circumferentially on the lee side. The force model incorporated a six-component internally mounted strain-gage balance and had an external contour identical to the pressure model. The support system hardware was the same for both models.

To study the effect of forced boundary-layer transition, the models were tested with and without a nose boundary-layer trip. The trip consisted of a 1/8-in.-wide circumferential strip or ring of No. 70 glass beads located from 1.75 to 2.8 in. aft of the nosetip for all the nose configurations tested.

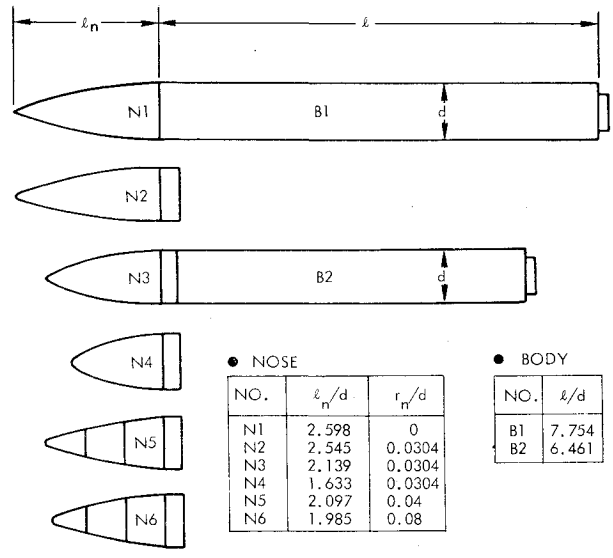

NO.	ℓ_n/d	r_n/d
N1	2.598	0
N2	2.545	0.0304
N3	2.139	0.0304
N4	1.633	0.0304
N5	2.097	0.04
N6	1.985	0.08

NO.	ℓ/d
B1	7.754
B2	6.461

Fig. 1 Model configuration and nomenclature.

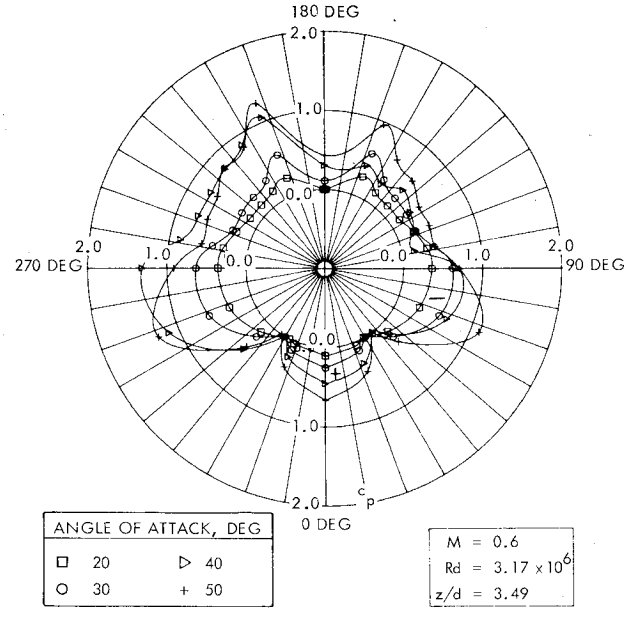

Fig. 2 Circumferential pressure distribution on N1B1.

Results and Discussion

Effect of Geometry on Side Force

The static pressure distribution on configuration N1B1 at station $z/d=3.49$ is presented in Fig. 2 at several angles of attack for $M=0.6$, $Rd=3.17\times10^6$. The pressures peaks at angles of 150°-160° and 200°-210° from the 0° windward meridian indicate the presence of vortex structures. At a 20° angle of attack, the pressure distribution is symmetric. For larger angles of attack, $\alpha=40°$ and $\alpha=50°$, asymmetric vortex development is indicated by the asymmetric pressure distribution.

The development of the asymmetric vortex structure and associated aerodynamic forces depends on specific missile nose geometry. Plots of the pressure distribution on configuration N2B1 (similar to N1B1 but with a slightly blunted nose) are practically symmetric, indicating that a slight amount of nose bluntness tends to alleviate asymmetric vortex development. Figure 3 is a plot of the side-force coefficient on N1B1 and N2B1 with angle of attack determined from the Phase III pressure tests. Although the N2B1 side-force magnitude is significantly affected by roll angle, the largest side-force coefficient is nevertheless obtained for the sharp ogive configuration N1B1.

Figure 4 is a plot of the N2B1 sectional side-force coefficient distribution obtained by pressure integration for the various roll angles at 40° angle of attack. Although roll angle significantly affects the side-force distribution, the normal force distribution was only slightly affected.

When comparing the side-force coefficient at angle of attack with fore-body geometry as a parameter, roll orientation should be varied because it is, in effect, a geometric parameter. In this investigation, limited roll angle data were obtained. Nevertheless, analyzing the available data for various grit-on and grit-off configurations and comparing the force test and pressure test results (physically, two different models) has led to some definite conclusions concerning the effect of forebody shape. Representative results are presented in Fig. 5. The smallest side force were obtained for the short ogive nose configuration N4B2 with slight bluntness. Triconic nose shapes produced side forces at least as large as similar fineness ratio ogives. It is evident from these results and from other sources[1-3] that increasing the nose fineness ratio results in an increase in maximum side-force coefficient, whereas slightly rounding the nose tends to decrease side force. Usually, decreasing the nose fineness ratio has a larger effect on reducing side force than does blunting the nose.

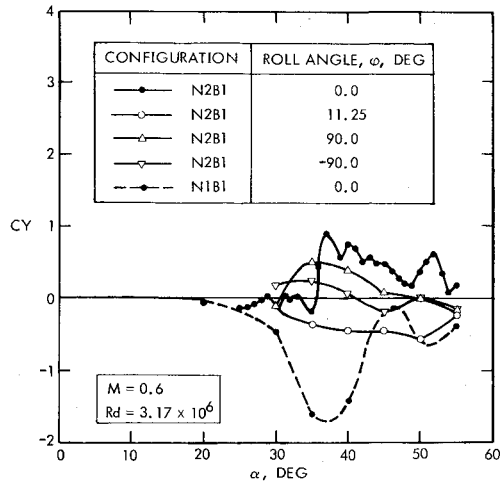

Fig. 3 Variation of side-force coefficient with roll angle.

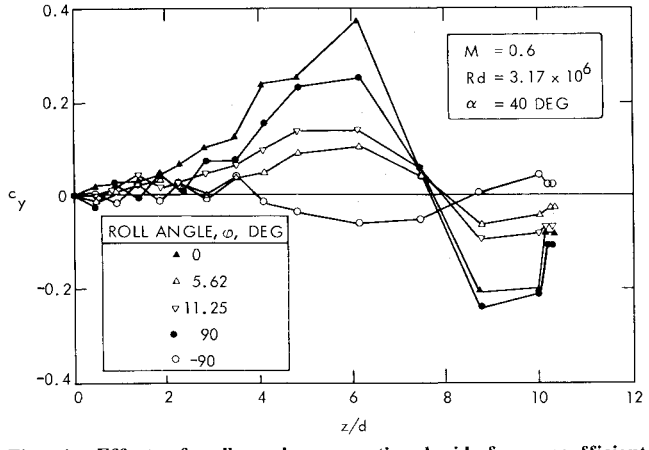

Fig. 4 Effect of roll angle on sectional side-force coefficient distribution on N2B1.

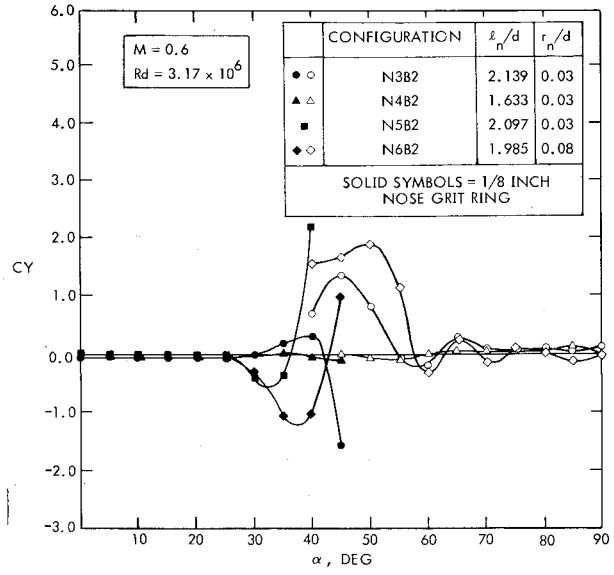

Fig. 5 Effect of nose shape on side force.

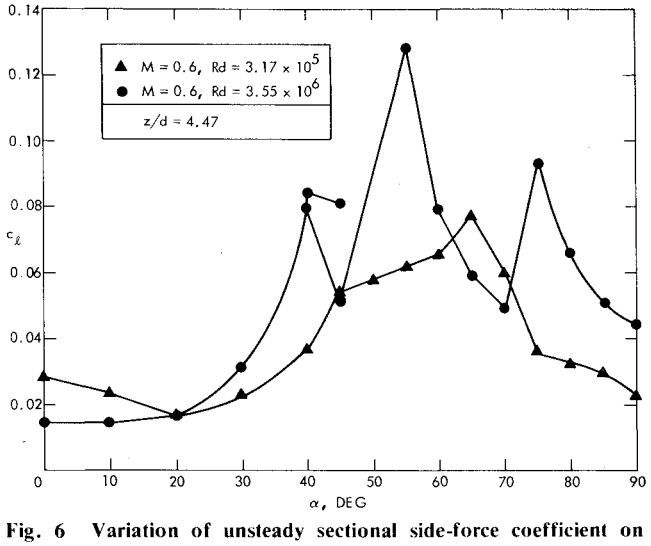

Fig. 6 Variation of unsteady sectional side-force coefficient on N2B1 with angle of attack.

No discernable trend in the data was found with respect to the model mounting, although large variations of side-force sign and magnitude were observed (Fig. 5). In general, the normal force variations were small.

Unsteady Side Force

For angles of attack greater than approximately 60°-70°, the vortices no longer remain attached to the body but are shed downstream in a manner similar to the classical vortex shedding behind a two-dimensional circular cylinder. There is no constant steady side force to present a control problem. However, oscillating side forces, if sufficiently intense or if they excite a sufficiently lightly damped elastic mode, can cause structural vibrations of the body, which can cause control instability, immediate structural failure, or fatigue failure.

Unsteady values of sectional side-force coefficient c_l were approximated in this investigation by integrating the rms unsteady component of pressure circumferentially around the missile. The results are presented in Fig. 6 at station $z/d=4.47$ where the most complete microphone data were obtained. The phase of the unsteady pressure was assumed such that maximum unsteady side force was calculated. On the windward side, where no unsteady pressure measurements were made, it was assumed that the pressures were small and of random phase.

For angles of attack less than 20°, the flow is essentially steady; unsteady pressures were on the order of the pressure fluctuations measured in the freestream, $(\Delta C_p)_{rms}=0.01$. The greatest unsteady pressures and unsteady side forces occurred for angles of attack between 30° and 70°. The large "steady" side forces observed by many investigations in this angle-of-attack range indicates that the detached vortices may fluctuate about some mean asymmetric configuration. At certain incidences, there may be more than one mean configuration. Under certain conditions, the vortex pattern was observed to rapidly switch from an almost symmetric configuration to a highly asymmetric one. This vortex-switching phenomenon was also noted by Clark and Nelson.[4] Maximum unsteady sectional side-force coefficient occurs between 55° and 65° angle of attack and then falls off as the angle of attack approaches 90°. The peak at $\alpha=75°$ for the $Rd=3.5\times10^6$ case corresponds to a 200 cps peak in the power spectral density plot for this station. Although for these test conditions 200 cps would correspond to a Strouhal shedding frequency of approximately $S=0.19$, cross correlation of the available microphone data did not indicate regular vortex shedding along the length of the missile.

Mach Number

Absolute values of the maximum side-force coefficient $|CY|_{max}$ for various test runs on N2B1 are presented in Fig. 7 as a function of Mach number for several values of Reynolds number. The data include side-force data measured directly in

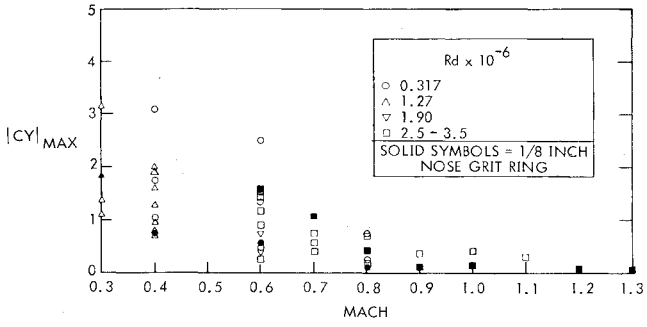

Fig. 7 Effect of Mach number on maximum side force coefficient on N2B1.

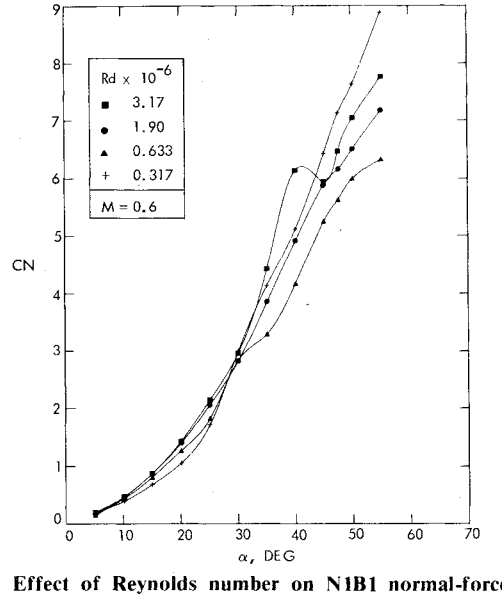

Fig. 8 Effect of Reynolds number on N1B1 normal-force coefficient.

the force tests, as well as values of side force as determined by integrating the pressure test data over the body surface. The maximum side-force coefficient for a given Mach number-Reynolds number condition varied at least with roll orientation, grit, and sting or strut mounting in the tunnel.

The magnitude of the side-force coefficient generally decreases with increasing Mach number and the maximum values occur at angles of attack between 35° and 55°. For Mach numbers greater than 0.8, the side-force coefficient is quite small. These results appear to be in agreement with the results of other investigators.[1-5]

The normal force coefficient increases with increasing Mach number up to $M=1.3$. More complete normal force and center of pressure data may be found in the AEDC test report.[6]

Effect of Reynolds Number

In Fig. 8, data are presented that show the effect of Reynolds number on N1B1 at $M=0.6$. For angles of attack less than 30°, the normal force increases with increasing Reynolds number. This trend continues up to a 90° angle of attack for supercritical and transcritical Reynolds number $Rd>5\times10^5$. For angles of attack greater than 30° (40° for $Rd=3.17\times10^6$), the largest normal force occurs for $Rd=3.17\times10^5$.

For angles of attack where the flow is assumed to be steady, the flow viewed in a cross-flow plane appears similar to the time development of the flow behind a two-dimensional circular cylinder started impulsively from rest. This similarity is the basis of the viscous cross-flow analogy, which states

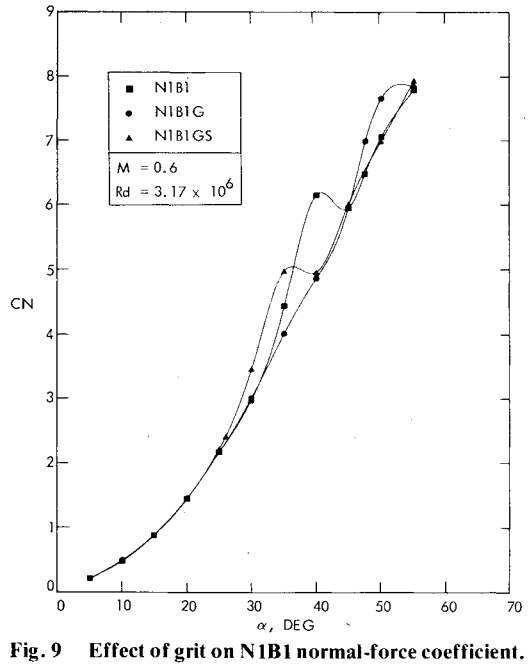

Fig. 9 Effect of grit on N1B1 normal-force coefficient.

what at any point along the missile the local normal force or side force may be replaced by the value of drag or lift, respectively, of the impulsively started cylinder at time $t=2z/d\tan\alpha$.

For Mach numbers $M\lesssim0.4$, cross-flow theory predicts the drag (missile normal force) should decrease and then increase as Reynolds number is increased from laminar subscritical flow, $Rd\sin\alpha<2\times10^5$, through transition to turbulence in the boundary layer, $Rd\gtrsim10^6$. For supercritical Mach numbers greater than $M=0.4$, the effect of Reynolds number on circular cylinder drag is less well defined. However, the current data indicate that a similar "drag bucket" exists for Mach numbers as great as $M=0.6$.

At a 40° angle of attack, cross-flow theory predicts greater normal force on N1B1 for $Rd=3.17\times10^5$ than for $Rd=3.17\times10^6$. The data in Fig. 8 indicate that this is not the case. One explanation is that axial flow still plays an important part and the cross-flow theory may not be completely valid, at least as far as the effect of Reynolds number on normal force is concerned. Smith and Nunn[7] have indicated that the apparent stall in the normal force curve, such as that at $\alpha=40°$ for $Rd=3.17\times10^6$, is a consequence of a transition from a flow dominated by the axial component to a flow in which cross-flow dominates. This can be seen in Fig. 9, which shows the effect of a ring of grit at the nose and strips of grit on N1B1 normal force. The ring of grit alone, N1B1G configuration, primarily affects the axial-flow and moves the stall point to a 55° angle of attack. When strips of grit at ±30° from the windward meridian were placed along the length of the body, N1B1GS configuration, the cross-flow was primarily affected and the stall point moved back to a 35° angle of attack. The no-grit stall point was $\alpha=40°$.

The effect of Reynolds number on side force is not as well defined as it is for normal force. The sensitivity of the asymmetric vortex development of roll orientation precludes a clear determination of the effect of Reynolds number on maximum side-force coefficient from the present data. For some cases, however, an apparent Reynolds number effect may be seen in the distribution of side force along the missile (Fig. 10). For the low Reynolds numbers, $Rd=3.17\times10^5$, the body vortices remain nearly symmetric for about half the missile length as indicated by the negligible sectional side-force coefficient. The vortices then become asymmetric as indicated by the large negative local side force. For the high Reynolds number run, $Rd=3.17\times10^6$, the vortices become

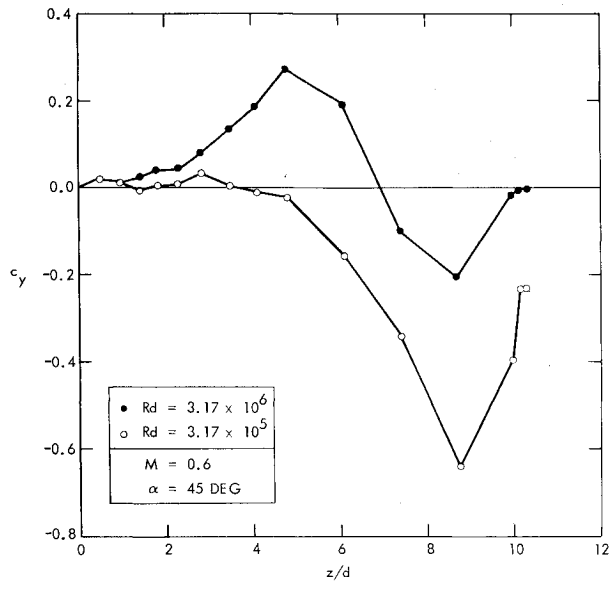

Fig. 10 Effect of Reynolds number on N2B1 side-force distribution.

asymmetric almost immediately. Using the cross-flow analogy to relate the axial distance z_s it takes for the local side-force coefficient to change sign to the corresponding change in sign of the time-dependent lift on the two-dimensional circular cylinder, it can be seen that increasing Reynolds number corresponds to an increase in cross-flow Strouhal number, i.e., $z_s/d=(2\ S\ \tan\alpha)^{-1}$. This is an agreement with high Reynolds number investigations of the shedding of vortices behind circular cylinders in which measurements have shown that the Strouhal number is increased over the subcritical Reynolds numbers case.

Theoretical Prediction Method

A method based on the unsteady cross-flow analogy has been developed by Marshall and Deffenbaugh[8] to calculate the flow about a body of revolution for moderate cross-flow Reynolds numbers $\Delta c<10^5$. The results presented in Ref. 8 are for angles of attack less than 25° and for symmetric flow.

The current work extends the method of Ref. 8 to high cross-flow Reynolds numbers, $10^6<Rc<10^7$, by using Stratford's criterion to predict the separation of the turbulent boundary layer. Angles of attack up to 40° are considered by allowing for asymmetric vortex development. Predictions of boundary-layer separation, asymmetric vortex development, normal and side forces, and load distributions on N1B1 at $M=0.6$, $Rd=3.17\times10^6$ are presented and are compared against the experimental values.

Basic Approach

Use of the cross-flow analogy reduces the complicated problem of the steady three-dimensional separated flow about a missile to the related two-dimensional problem of a circular cylinder started impulsively from rest whose radius changes with time. The time-dependent lift and drag has not been determined experimentally for this problem.

A solution to the problem is obtained by assuming that for high Reynolds numbers the flow may be divided into two regions: a viscous inner flow near the cylinder and an essentially inviscid outer flow elsewhere. The outer flow consists of the classical potential flow around a circular cylinder superimposed with the potential flow of a number of ideal point vortices which describe the wake. The inner flow consists of a boundary layer and a rear shear layer and is the source of the outer flow vorticity. The rear shear layer accounts for vorticity created over the rear portion of the cylinder by the backflow induced by the main vortex structure. The opposite signed vorticity generated from the rear shear layer has the effect of reducing the vortex strength in the wake over that shed from the boundary layer.

The point vortices are fed into the wake at the separation points and are then allowed to move with the fluid. The strength of the point vortices are obtained by summing the vorticity flux out of the boundary layer or rear shear layer over a time step Δt, i.e., $\Gamma=\Delta t(u^2/2)$. The outer potential flow is continually modified by the movement of the point vortices and by the introduction of new point vortices into the wake. The outer potential flow provides the boundary conditions for the boundary-layer solution which results in updated values of separation angle.

Similar discrete vortex wake methods have been developed by Angelucci[9] and by Wardlaw,[10] but they specify the points of separation empirically and do not account directly for vorticity created over the rear of the cylinder. In this work, Stratford's criterion is used to determine the boundary-layer separation points; rear shear-layer separation is a function of the pressure distribution obtained from the outer flow and the boundary-layer separation angle.

Turbulent Separation

Stratford[11] devised a method to determine the separation point of a turbulent bounday layer from an arbitrary pressure distribution. At Reynolds numbers of $10^6<R<10^7$ turbulent separation occurs at $\bar{x}$ when

$$(2C_p)^{5/4}\left(\bar{x}\frac{dC_p}{d\bar{x}}\right)^{1/2}=1.06\beta(10^{-6}R)^{1/10} \tag{1}$$

where $R=$Reynolds number based on local value of equivalent distance, $\bar{x}$, and peak velocity, u_m, or velocity at transition, u_{tr}, whichever occurs later. The equivalent distance, $\bar{x}$, accounts for an initial region of favorable pressure gradient and for a boundary layer which is initially laminar. Following Stratford's derivation

$$\bar{x}=\bar{x}-\bar{x}_0+\bar{x}_s+38.2(u_0/u_{tr})^{1/8}(Rtr)^{-3/8}$$

$$\left[\int_{\bar{x}_s}^{\bar{x}_{tr}}\left(\frac{u}{u_0}\right)^5 d\bar{x}\right]^{5/8}\left(\bar{x}_{tr}\right)^{3/8}+\int_{\bar{x}_{tr}}^{\bar{x}_0}\left(\frac{u}{u_0}\right)^3 d\bar{x} \tag{2}$$

where

$$u_0=u_m=u(\bar{x}_m)\qquad \bar{x}_0=\bar{x}_m\qquad \bar{x}_m>\bar{x}_{tr} \tag{3a}$$

$$u_0=u_{tr}=u(\bar{x}_{tr})\qquad \bar{x}_0=\bar{x}_{tr}\qquad \bar{x}_m<\bar{x}_{tr} \tag{3b}$$

The empirical factor $\beta=0.73$.

In the current method, C_p and $dC_p/d\bar{x}$ are calculated from the outer potential flow solution using Bernoulli's equation, and separation is determined from Eq. (1). Implicit in the use of Eq. (1) is the assumption of a quasisteady flow.

For flow close to the missile nose, which corresponds to times shortly after impulsive start, the time-dependent terms are important for the circular cylinder solution and must be included. In the present method, the unsteady laminar boundary-layer equations are solved using finite differences[12] to determine separation for distances within $Z_n/d=1.0/2\tan\alpha$ of the nose apex. Aft of Z_n/d on the missile, the boundary layer on the corresponding circular cylinder ($t>1.0$) is close to steady state which allows for a quasisteady approximation and use of Stratford's separation criterion, Eq. (1). As pointed out by Smith and Nunn,[7] near the apex of the nose the cross-flow Reynolds number is low (small body diameter) and separation may be laminar even though cross-flow Reynolds number based on after-body diameter indicates turbulent separation. Also, as pointed out by Thomson,[13] the favorable pressure gradient over the nose may inhibit transition to some extent.

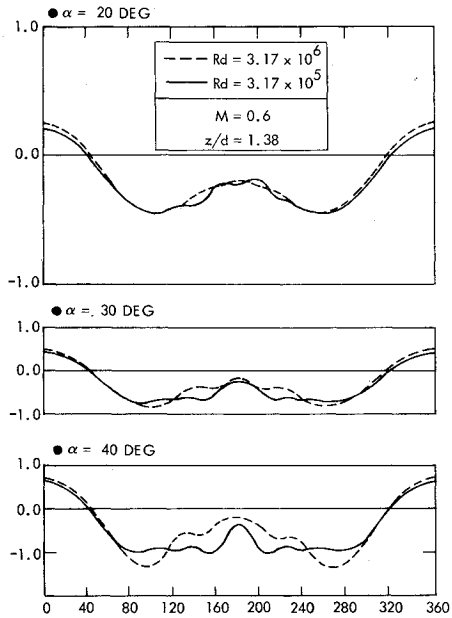

Fig. 11 Experimental circumferential pressure distribution on N2B1.

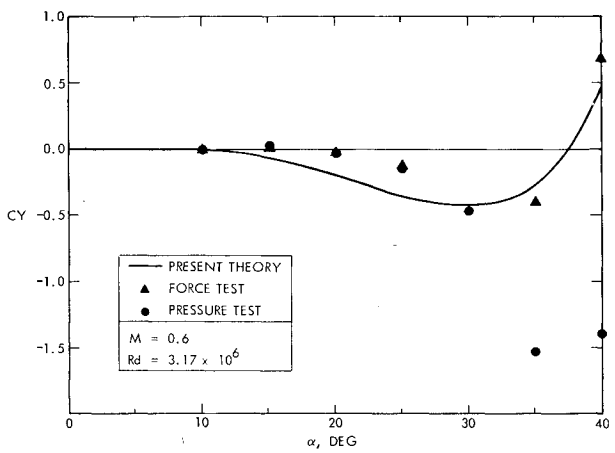

Fig. 12 Effect of angle of attack on N1B1 side-force coefficient.

The pressure distribution at station $z/d=1.38$ is presented in Fig. 11 for $\alpha=20°$, 30°, 40° for $Rd=3.17\times10^5$ and 3.17×10^6. If it can be assumed that the low Reynolds number distribution represents a laminar separation, it is clear that turbulent separation occurs for 30° and 40° angle of attack for the high Reynolds number case $Rd=3.17\times10^6$ at this station. For 40°, similar results indicated turbulent separation as close as $z/d=0.46$ from the nose apex.

For angles of attack less than 20°, the pressure profiles are similar for $Rd=3.17\times10^5$ and $Rd=3.17\times10^6$ at $z/d=1.38$ indicating a laminar separation. While the current assumption of a laminar boundary near the nose is valid for angles of attack less than 20°, for higher angles of attack it may be necessary to solve the unsteady turbulent boundary-layer equations to determine separation for high Reynolds number flows $Rd>10^6$.

Results

Ideally, for a symmetric body, the vortices will continue to grow symmetrically. However, it is well-known that at high Reynolds numbers the symmetric vortex structure is inherently unstable and a small perturbation will lead to the development of an asymmetric wake. Numerous investigators have hypothesized that small irregularities in the machining of the missile nose perturb the symmetric vortex development. In the current solution scheme, this perturbation was modeled by reducing by 10 percent the vorticity flux out of the boundary layer along one side of the missile nose.

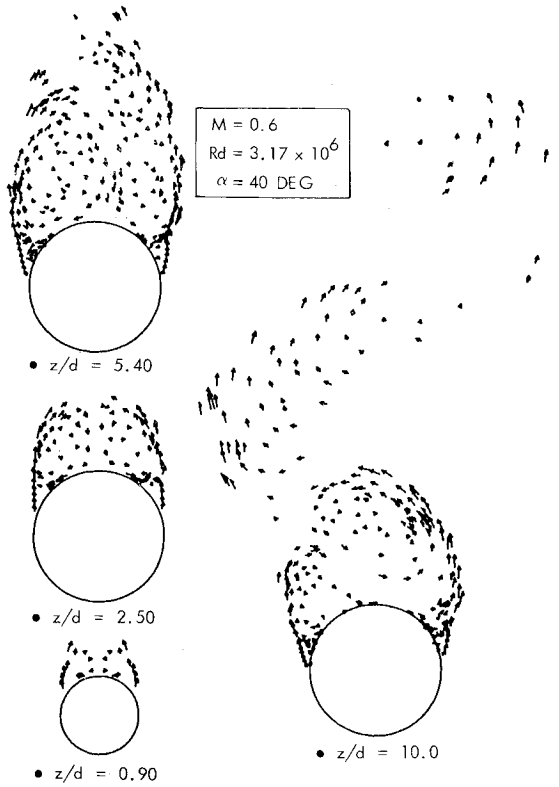

Fig. 13 Theoretical asymmetric vortex development on N1B1.

The predicted angle of attack of side force onset, Fig. 12, is 20°. Experimentally, the side force first becomes significant at approximately 25° angle of attack. Good agreement with the force test data is obtained for the higher angles of attack. The predicted side force coefficient changes sign between 30° and 40° as does the force test data. The predicted change in sign is caused by an additional vortex being shed at 40°. The experimental pressure data indicates a much larger side force at 35° and 40° and does not change sign. Experimentally, it has not been clearly determined whether the change in sign is due to the addition of another vortex or the possible complete switching of the asymmetric vortex structure.

Figure 13 is a plot of the development of the wake looking upstream. The theoretical side force coefficient distribution is presented in Fig. 14. As shown in Figs. 13 and 14, little asymmetry is apparent until after $z/d=2.5$. At $z/d=5.40$, vorticity from the left vortex has been entrained into the right vortex which elongates and weakens. The local side-force distribution reaches a maximum negative value at this point. As the left vortex grows stronger, it draws the right-feeding shear layer across the wake cutting off further supply of vorticity to the right vortex, which is then shed. The left vortex grows weaker as a new right vortex begins to form and the side-force distribution changes sign. At the last station, $z/d=10.0$, the growing right vortex has just entrained the left shear layer, shedding a left vortex as the process begins to repeat itself. The first vortex shed is noticeably weaker than the second.

Although the station at which the local maximums occur is well predicted (Fig. 14), the magnitude of the local side-force coefficient at $z/d=5.0$ is only about a third of the experimental value. As pointed out earlier, the experimental side-force coefficient distribution is highly dependent on roll angle, but the local maximum values tend to occur at approximately the same station, and the magnitude is generally larger over the forward part of the missile (Figs. 4 and 14).

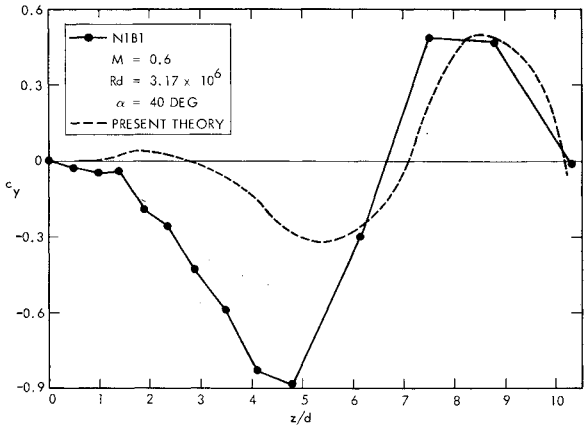

Fig. 14 Sectional side-force coefficient distribution on N1B1.

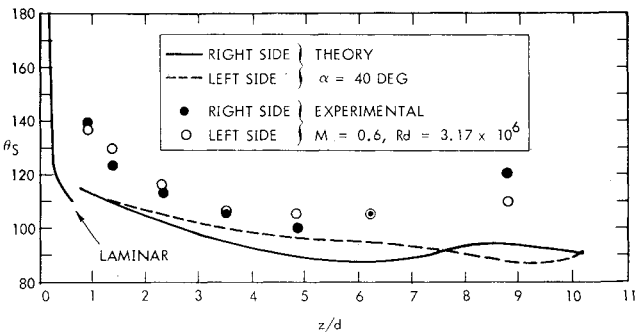

Fig. 15 Separation angle looking upstream.

The cross-flow analogy may have to be re-examined in light of these results, because the impulsive start circular cylinder solution predicts ocillatory lift values of approximately equal magnitude.

The prediction of separation lines along N1B1 at a 40° angle of attack are presented in Fig. 15. Experimental values of separation were estimated as the point where the pressure distribution flattens out after encountering an adverse pressure gradient. Based on current best estimates from the pressure distributions, the use of Stratford's separation criterion with the discrete vortex-wake model predicts early separation by about 15%. In the present method, it was implicitly assumed that by using Stratford's method to predict turbulent separation, the turbulent wake would be correctly modeled; the elementary point vortex strengths being affected by the location of separation. Further modification of the discrete vortex wake model may be required to account for turbulence effects in the wake, perhaps through the use of an empirical factor to adjust the point vortex strengths. Also, potential for improving the accuracy of the method exists by determining the Stratford's empirical factor β from the present experimental transcritical Reynolds number ($Rd > 10^6$) data.

Conclusions

Selected results from an extensive wind-tunnel program have been presented. Several ogive and triconic bodies of varying fineness and bluntness ratios were tested. Force and moment data and surface pressure distributions were obtained over a wide range of Mach numbers and Reynolds numbers. Unsteady pressure data and high transcritical Reynolds number data at Mach 0.6 had not been previously obtained for this problem.

From analysis of the data obtained in this study, the following can be concluded:

1) For angles of attack between 30° and approximately 70° the three-dimensional flow becomes quasisteady. The largest unsteady side forces occur in this region. The large "steady" side forces that occur from a 35° to 55° angle of attack indicate that the detached vortices fluctuate about some mean asymmetric configuration.

2) Side force is very sensitive to small changes in roll angle. The magnitude of maximum side-force coefficient decreases with decreasing nose-fineness ratio and the introduction of bluntness. The side forces for triconic nose shapes are at least as large in magnitude as similar fineness/bluntness ratio ogives.

3) The largest side-force coefficients occur for Mach numbers less than 0.6 and are negligible for Mach >0.8. For transcritical Reynolds number flow and angles of attack greater than 30°, turbulent separation occurs very close to the nose apex. The effect of increasing Reynolds number on side-force distribution can be explained in terms of an increasing cross-flow Strouhal number.

An analytical method based on the unsteady cross-flow analogy was developed to predict the flow about slender missiles at angles of attack up to 40° for transcritical cross-flow Reynolds numbers. Comparison of the predicted side-force coefficient with the experimental data is difficult due to the roll sensitivity. At a 40° angle of attack, the cross-flow theory predicts a lower side force load over the forward part of the missile than that observed experimentally.

Whereas some agreement with experiments is obtained using the discrete vortex wake cross-flow analogy and potential for improvement exists in the modeling of the turbulent wake, it is felt that a general solution to the problem can only be obtained by considering the complete three-dimensional flow. The current technique is useful because it provides a means to understand further the physics of a complicated problem and because it may provide useful information (such as vortex positions and strengths for simpler design techniques.

Acknowledgment

The authors gratefully acknowledge the efforts by Maj. L. A. Vancura (SAMSO), M. Buck, and D. Shereda (AFFDL) involving test management, model design and fabrication, test planning and conductance, and final data reduction and plotting. The efforts of D. Baker and D. Reichenau (ARO) during the conductance of the test are also greatly appreciated. This work was paritally supported under SAMSO Contract F04704-75-0029.

References

[1] Jorgensen, L. H. and Nelson, E. R., "Experimental Aerodynamic Characteristics for a Cylindrical Body of Revolution with Various Noses at Angles of Attack from 0° to 58° and Mach Numbers from 0.6 to 2.0," NASA TM X-3128, Dec. 1974.

[2] Pick, G. S., "Side Forces on Ogive-Cylinder Bodies at High Angles of Attack in Transonic Flow," *Journal of Spacecraft and Rockets*, Vol. 9, June 1972, pp. 398-390.

[3] Keener, E. R. and Chapman, G. T., "Onset of Aerodynamic Side Forces at Zero Sideslip on Symmetric Forebodies at High Angles of Attack," AIAA Paper 74-770, Anaheim, Calif., 1974.

[4] Clark, W. C. and Nelson, R. C., "Body Vortex Formation on Missiles at High Angles of Attack," AIAA Paper 76-65, Washington, D. C., 1976.

[5] Fleeman, E. L. and Nelson, R. C., "Aerodynamic Forces and Moments on a Slender Body with a Jet Plume for Angles of Attack up to 180 Degrees," AIAA Paper 74-110, Washington, D. C., 1974; also *Journal of Spacecraft and Rockets*, Vol. 12, Jan. 1975, pp. 12-16.

[6] Baker, D. C. and Reichenau, D. E. A., "Aerodynamic Characteristics of an MX Missile at Free-Stream Mach Numbers from .3 to 1.3 and Angles of Attack up to 180 Degrees," Arnold Engineering Development Center, Arnold AFB, Tenn, AEDC-TR-75-34, April 1975.

[7] Smith, L. H. and Nunn, R. H., "Aerodynamic Characteristics of an Axisymmetric Body Undergoing a Uniform Pitching Motion," *Journal of Spacecraft*, Vol. 13, Jan. 1976, pp. 8-14.

[8] Marshall, F. J. and Deffenbaugh, F. D., "Separated Flow Over a Body of Revolution," *Journal of Aircraft*, Vol. 12, Feb. 1975, pp. 78-85.

[9]Angelucci, S. B., "A Multivortex Method for Axisymmetric Bodies at Angle of Attack," *Journal of Aircraft*, Vol. 12, Dec. 1971, pp. 959-966.

[10]Wardlaw, A. B., Jr., "Multivortex Model of Asymmetric Shedding on Slender Bodies at High Angles of Attack," AIAA Paper 75-123, Washington, D. C. 1975.

[11]Stratford, B. S., "The Prediction of Separation of the Turbulent Boundary Layer," *Journal of Fluid Mechanics*, Vol. 5, Jan. 1959, pp. 1-16.

[12]Hall, M. G., "A Numerical Method for Calculating the Unsteady Two Dimensional Laminar Boundary Layer," *Ingenieur-Archivum* Vol. 38, 1969, pp. 97-106.

[13]Thomson, K. D., "The Estimation of Viscous Normal Force, Pitching Moment, Side Force and Yawing Moment on Bodies of Revolution of Incidences up to 90°," Australian Defense Scientific Services, Melbourne, Australia, WRE-Rep. -782 (WR&D), Oct. 1972.